

# Strain-induced isosymmetric phase transition in BiFeO<sub>3</sub>

Alison J. Hatt and Nicola A. Spaldin

Materials Department, University of California, Santa Barbara, CA 93106-5050

Claude Ederer

School of Physics, Trinity College, Dublin 2, Ireland

(Dated: July 23, 2021)

We calculate the effect of epitaxial strain on the structure and properties of multiferroic bismuth ferrite, BiFeO<sub>3</sub>, using first-principles density functional theory. We investigate epitaxial strain corresponding to an (001)-oriented substrate and find that, while small strain causes only quantitative changes in behavior from the bulk material, compressive strains of greater than 4% induce an isosymmetric phase transition accompanied by a dramatic change in structure. In striking contrast to the bulk rhombohedral perovskite, the highly strained structure has a  $c/a$  ratio of  $\sim 1.3$  and five-coordinated Fe atoms. We predict a rotation of polarization from [111] (bulk) to nearly [001], accompanied by an increase in magnitude of  $\sim 50\%$ , and a suppression of the magnetic ordering temperature. Our calculations indicate critical strain values at which the two phases might be expected to coexist and shed light on recent experimental observation of a morphotropic phase boundary in strained BiFeO<sub>3</sub>.

## I. INTRODUCTION

BiFeO<sub>3</sub> (BFO) has been widely studied for its room temperature multiferroic properties, in which the electric polarization is coupled to antiferromagnetic order, allowing for manipulation of magnetism by applied electric fields and vice versa<sup>1-5</sup>. In its bulk form, BFO occurs in the  $R3c$  space group<sup>6</sup>, but it is often studied in the form of thin films where it is subject to an epitaxial constraint. Such constraints impose coherency and strain that in general distort the bulk structure and/or stabilize phases not present in the bulk material<sup>7-9</sup>. Indeed, several groups have reported stabilization of a nearly tetragonal phase in highly strained BFO films grown on LaAlO<sub>3</sub> substrates with a giant  $c/a$  ratio close to 1.3<sup>10,11</sup>. A similar result was found by earlier theoretical studies that constrained BFO to tetragonal  $P4mm$  symmetry, thus preventing the rotational distortions found in the  $R3c$  bulk phase<sup>12,13</sup>. Within this constraint the theoretical ground state of BFO has a massively reduced in-plane lattice parameter of 3.67Å and a “super-tetragonal” unit cell with  $c/a=1.27$ . This  $P4mm$ -constrained structure has an enhanced polarization roughly 1.5 times that of the bulk single crystal, a remarkable increase that has also been reported experimentally, though not widely reproduced<sup>14</sup>. Lisenkov *et al.* recently used model calculations to suggest that the  $P4mm$  phase can also be stabilized by electric fields, and they identified an additional phase intermediate to the strained-bulk phase and  $P4mm$  induced by application of a [001] electric field<sup>15</sup>. The most recent experimental results, from Béa *et al.* and Zeches *et al.*, have resoundingly confirmed the existence of a second phase with giant  $c/a$  in BFO thin films grown on (001) LaAlO<sub>3</sub> but suggest a monoclinically distorted space group  $Cc$ <sup>10,11</sup>. In contrast to earlier experimental studies, Béa *et al.* only found a modest enhancement of the polarization. Intriguingly, Zeches *et al.* observed the coexistence of the high strain “super-tetragonal” phase and a low strain bulk-like phase with defect- and dislocation-free interfaces between phase domains, in spite of a large difference in out-of-plane lattice parameters.

In this work we use ab initio calculations to investigate

the effect of epitaxial strain on BFO without the additional imposed symmetry constraints used in earlier first-principles studies. We address the most widely used (001)-oriented cubic substrates and cover a range of strains encompassing all experimentally accessible states. Our calculations reveal a strain-induced phase transition at  $\sim 4.5\%$  compressive strain, consistent with recent experimental reports<sup>10,11</sup> and in addition show that the transition is *isosymmetric*. We reported these basic results in Ref. 11, and in the present work we provide the complete theoretical background and analysis. Our analysis of the isosymmetric behavior in the transition region suggests an explanation for several experimental results reported in Ref. 11; namely, the coexistence of bulk-like and super-tetragonal phases in films grown on LaAlO<sub>3</sub> substrates, and the reversible movement of domain walls in these same films by electric field. In addition, our calculations of the magnetic properties of the super-tetragonal phase point to magnetic behavior that is distinct from the rhombohedral phase. Finally, in the low strain regime, we confirm that epitaxial strain has only a small quantitative effect on the properties of rhombohedral BFO<sup>12</sup>.

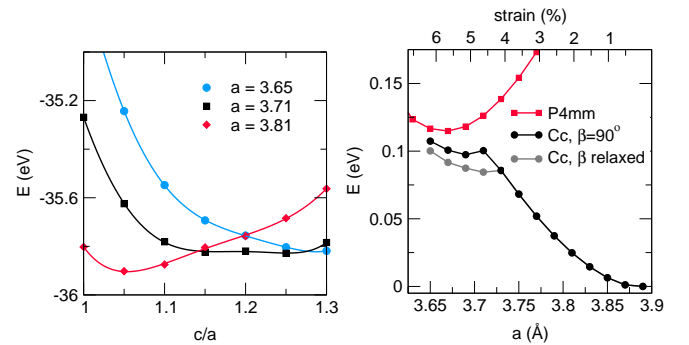


FIG. 1: *Left*: Total energy per formula unit as a function of  $c/a$  ratio for three constrained  $a$  parameters. *Right*: Energy per formula unit relative to bulk BFO for the ground state structures as a function of  $a$  for  $P4mm$ , un-relaxed monoclinic angle ( $\beta=90^\circ$ ), and relaxed monoclinic angle.

## II. COMPUTATIONAL METHOD

We perform density functional calculations using the local spin density approximation plus Hubbard  $U$  (LSDA+ $U$ ) approach as implemented in the software package VASP<sup>16</sup>. We use an effective  $U$  of 2 eV, which has been shown to give a good description of bulk properties of BFO<sup>1</sup>. We use the projector augmented wave method<sup>17</sup>, the default VASP potentials (Bi\_d, Fe\_pv, O), a  $5 \times 5 \times 5$  Monkhorst-Pack k-point mesh, and a 500 eV energy cutoff. Spin-orbit coupling is not included in these calculations and unless otherwise noted we impose the bulk G-type antiferromagnetic order. Electric polarization is calculated using the Berry phase method<sup>18,19</sup>.

To address the effect of epitaxial strain, we use a 10 atom unit cell with lattice vectors  $\vec{a}_1 = (a, a, 0)$ ,  $\vec{a}_2 = (\Delta, a + \Delta, c)$ , and  $\vec{a}_3 = (a + \Delta, \Delta, c)$ . This unit cell can accommodate the alternating rotations of the FeO<sub>6</sub> octahedra found in the bulk  $R3c$  structure, while enforcing the formation of a square lattice within the  $x$ - $y$  plane, corresponding to the epitaxial constraint imposed by a (001) oriented cubic substrate with in-plane lattice constant  $a$ . Furthermore, it allows us to relax the out-of-plane lattice parameter  $c$  and a possible monoclinic tilt  $\beta$  of the pseudo-cubic perovskite unit cell ( $\tan \beta = c/\Delta$ ). For  $a = c = 3.89$  Å and  $\Delta = 0$  one obtains the lattice vectors of the relaxed  $R3c$  structure of bulk BFO, albeit with the rhombohedral angle fixed to 60°. Note that since the relaxed value of this angle for  $U_{\text{eff}} = 2$  eV is 59.99° (see Ref. 1) this is barely a constraint. For computational simplicity we first consider the case  $\Delta = 0$ , i.e. no monoclinic distortion of the perovskite unit cell ( $\beta = 90^\circ$ ); this constraint is relaxed later.

## III. RESULTS AND DISCUSSION

### A. Energetics and Structure

We start by examining how the energy varies with out-of-plane lattice parameter for strained BFO. For in-plane lattice parameters corresponding to compressive strains up to 6.2% we vary  $c/a$  and, for each  $c/a$  value, we relax all internal coordinates until the Hellman-Feynman forces are no larger than 1 meV/Å on any atom. The internal coordinates are initialized according to the relaxed bulk  $R3c$  structure, resulting in space group symmetry  $Cc$ . Fig. 1(left) shows the resulting total energy as a function of  $c/a$  for three representative cases. For  $a = 3.81$  Å, corresponding to a moderate compressive strain of 2.06 % relative to the LSDA bulk value (3.89 Å), a single energy minimum is observed at  $c/a \sim 1.05$ , i.e. relatively close to unity. For  $a = 3.65$  Å, i.e. 6.17 % compressive strain, we again find a single energy minimum, but this time at a very large  $c/a$  of almost 1.3. In contrast, for an intermediate value of  $a = 3.71$  Å (4.63 % compressive strain), the energy curve is almost flat between  $c/a \sim 1.1$  and 1.3. Our calculations indicate the presence of two minima at this intermediate  $a$ , a global minimum at large  $c/a \approx 1.25$  and a local minimum at smaller  $c/a \approx 1.15$ . Further calculations would be required to fully resolve the energy curve in this region.

We then use polynomial fits to extract the value of  $c/a$  that

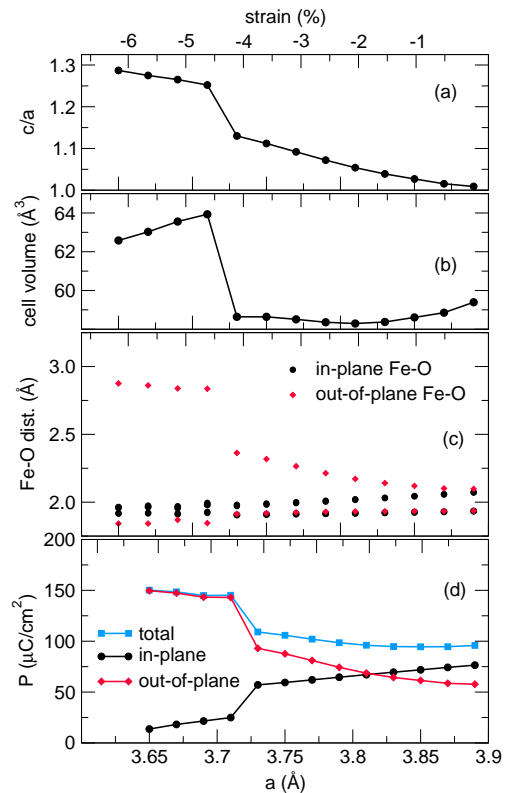


FIG. 2: Structural parameters as functions of lattice parameter/strain relative to the bulk LSDA+ $U$  lattice parameter. (a)  $c/a$  of the pseudo-cubic cell; (b) volume per formula unit; (c) Fe-O bond lengths for in-plane and out-of-plane bonds; (d) total polarization and components lying in-plane and out-of-plane. All values are for constrained monoclinic angle,  $\beta=90^\circ$ .

minimizes the total energy for fixed  $a$ , and relax all atoms again at the obtained  $c/a$  ratio, still maintaining  $\beta = 90^\circ$ . The total energy of the resulting structures is shown in Fig. 1 (right), relative to the energy of bulk  $R3c$ . The corresponding evolution of various structural parameters ( $c/a$  ratio, unit cell volume, Fe-O distances) and of the electric polarization as a function of strain is shown in Fig. 2. All of these quantities exhibit a sharp discontinuity between  $a = 3.71$  Å and  $a = 3.73$  Å, i.e. 4-4.5% strain, where also the total energy depicted in Fig. 1 (right) has a kink, indicative of a first-order phase transition.

Finally, we perform additional total energy calculations for  $\beta \neq 90^\circ$ , determine the optimal  $\beta$  for each value of  $a$  from a polynomial fit, and again relax atom positions within this new unit cell. For  $a < 3.72$  Å we find a monoclinic distortion of the unit cell of  $\sim 1^\circ$  to  $2^\circ$  that reduces the energy by 10 meV/f.u. compared to  $\beta = 90^\circ$ , as shown in Fig. 1. The resulting atomic configuration represents only a minor structural change from the  $\beta=90^\circ$  case and we thus neglect this distortion in all further calculations, only reporting results for  $\beta=90^\circ$ .

We start our discussion by first characterizing the structures for two extreme cases representative of the small and large strain regimes,  $a = 3.85$  Å and  $a = 3.65$  Å,  $\sim 1\%$  and  $6\%$  compressive strain, respectively. At 1% strain the relaxed structure

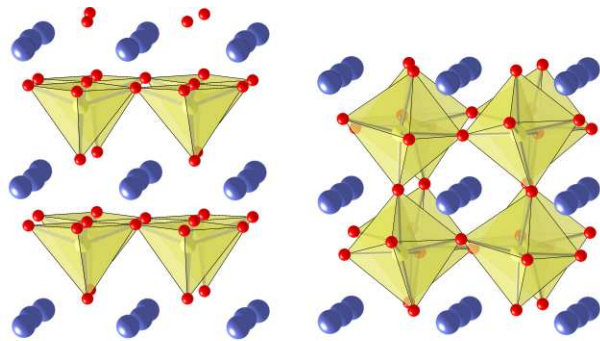


FIG. 3: Isosymmetric phases of  $Cc$  BFO: *Left*: tetragonal-like  $T$ -phase; *Right*: rhombohedral-like  $R$ -phase.

closely resembles the rhombohedral  $R3c$  bulk phase, but the epitaxial constraint causes a monoclinic distortion that lowers the symmetry from  $R3c$  to  $Cc$ . The corresponding structure is depicted in Fig. 3 (right). Following the notation introduced in Ref. 11, we call this the ‘ $R$ ’ phase to emphasize its similarity to the rhombohedral parent phase. The internal structure remains similar to the unstrained bulk, with octahedrally coordinated Fe, a ferroelectric distortion consisting of ionic displacements along the pseudocubic (PS)  $[111]$  axis, and antiferrodistortive rotations of the  $\text{FeO}_6$  octahedra around  $[111]_{\text{PS}}$ . The  $[001]_{\text{PS}}$  component of the antiferrodistortive rotation increases and the  $[110]_{\text{PS}}$  component decreases as we shrink the in-plane lattice constant, but no qualitative change occurs for compressive strains up to 4%. The electric polarization, constrained by symmetry to lie within the monoclinic glide plane, is almost entirely along  $[111]_{\text{PS}}$ , rotating slightly towards  $[001]_{\text{PS}}$  as compressive strain is increased (see Fig. 2d). Our results are consistent with the growing body of literature on BFO under moderate compressive strain<sup>11,20,21</sup>

At 6% strain, the ground state resembles the  $P4mm$  structure described previously for tetragonally-constrained BFO<sup>22</sup>. Using the notation from Zeches *et al.*<sup>11</sup>, we refer to the high-strain structure as the ‘ $T$ ’ phase for its similarity to tetragonal  $P4mm$ . The Fe undergoes large displacement towards one of the apical oxygens (see Fig. 2c), resulting in a “super-tetragonal” structure with five-coordinated Fe, similar to the coordination of the transition metals in perovskites  $\text{PbVO}_3$  and  $\text{BiCoO}_3$ <sup>23,24</sup> (see Fig. 3).  $P4mm$  symmetry is broken by antiferrodistortive tilting of the square-pyramidal oxygen cages (analogous to octahedral tilt) around  $[110]_{\text{PS}}$  by  $5.1^\circ$ . Interestingly, the  $T$  phase does not exhibit the  $[001]_{\text{PS}}$  rotations that have been associated with compressive strain in other perovskites<sup>25,26</sup>. This is likely associated with the change in Fe coordination, which encourages displacement along  $[001]_{\text{PS}}$  in response to decreased lattice parameter rather than rotation of the oxygen cages.

As can be seen in Fig. 1 (right), the  $T$  phase is significantly lower in energy than  $P4mm$ . Furthermore, it follows from Fig. 1 that at about 5% strain the energy reduction obtained by allowing the tiltings (going from  $P4mm$  to  $Cc$  at  $\beta = 90^\circ$ ) is even larger than the subsequent reduction from relaxing  $\beta$ . These results indicate that the formation of a tetragonal  $P4mm$

phase in BFO films grown on  $\text{SrTiO}_3$  substrates, as reported e.g. in Ref. 14, is highly unlikely.

The polarization vector is within the glide plane, as in the low strain regime, but is now strongly rotated to be almost entirely out-of-plane, along  $[001]_{\text{PS}}$  (Fig. 2d). In addition, the magnitude (relative to a  $Pm\bar{3}m$  reference structure) increases from  $96 \mu\text{C}/\text{cm}^2$  in the unstrained bulk to  $150 \mu\text{C}/\text{cm}^2$ . This is in contrast to the modest enhancement reported in Ref. 10, where a remnant polarization of  $75 \mu\text{C}/\text{cm}^2$  is reported for Mn-doped films on  $\text{LaAlO}_3$  substrates, compared to  $60 \mu\text{C}/\text{cm}^2$  in bulk<sup>27</sup>. The discrepancy in enhancement might be a result of the 5% Mn doping used to reduce current leakage but it could also indicate incomplete switching of the polarization. This is reasonable, as we expect the large distortion accompanying the polarization to be associated with a large coercivity. Reorientation of the out-of-plane polarization would require a significant change in bonding for the 5-coordinated structure and it is possible that the nature of switching is quite different in the super-tetragonal phase than in the bulk.

We observe that the total polarization  $\vec{P}$  is nearly constant within the low strain regime (1%–2%) but that the out-of-plane projection grows at the expense of the in-plane projection (Fig. 2d). This is in part associated with the growing  $c/a$ , but when we correct for that we find that  $\vec{P}$  is rotated toward the  $[001]$  direction by several degrees at -1% strain. This rotation in the low strain regime is qualitatively similar to that reported in Ref. 28, although we find a much smaller enhancement of the total polarization. The rotation across the transition from  $R$  to  $T$  is much larger: at  $a = 3.73 \text{ \AA}$  the angle between  $\vec{P}$  and  $[001]$  is  $31.52^\circ$ ; at  $a = 3.71 \text{ \AA}$  it is  $9.90^\circ$ . We suspect that this dramatic rotation is responsible for the recently demonstrated ability to shift the phase boundary with an electric field in BFO films with mixed  $T$  and  $R$  phases<sup>11</sup>. An electric field applied along  $[001]$  will favor an out-of-plane polarization, thus growing the  $T$  phase at the expense of  $R$ . The properties that are responsible for the side-by-side coexistence of  $T$  and  $R$  domains, and for the reversible nature of this domain shifting, are addressed later.

## B. Octahedral Modes

To further quantify the phase transition, we decompose the structural distortion relative to a  $P4/mmm$  reference structure into symmetry irreducible modes using the ISODISPLACE software<sup>29</sup>. We find the largest changes as a function of strain in the antiferrodistortive  $A_{4-}$  and  $A_{5-}$  modes (see Fig. 4). These modes correspond to alternating rotations of the  $\text{FeO}_6$  octahedra around the  $[001]_{\text{PS}}$  and  $[110]_{\text{PS}}$  axes, respectively, and are therefore a measure of the octahedral rotations and tilts, similar to the analysis presented in previous work<sup>25,26</sup>. In fact, the dependence of rotation and tilt angles (using the terms as defined in Ref. 25) on lattice parameter are qualitatively identical to those of the corresponding symmetry adapted modes. As can be seen from Fig. 4, the transition between  $T$  and  $R$  phases can be characterized by the evolution of the  $A_{4-}$  and  $A_{5-}$  modes as a function of lattice parameter, which

again exhibit pronounced discontinuities around  $a = 3.71 \text{ \AA}$ . In particular, the  $A_{4-}$  mode vanishes in the  $T$  phase. This suggests that the isosymmetric phase transition is related to the stability of the corresponding phonon mode, which is unstable for larger in-plane lattice parameters whereas it becomes stable for large compressive in-plane strain. The phase transition thus seems to be of similar microscopic origin as conventional soft mode transitions, albeit with no resulting change in space group symmetry.

### C. Magnetic Coupling

Finally, we calculate the relative energies of likely magnetic orderings in the  $T$  phase. We double the unit cell to allow A- and C-type orderings and re-relax the atom positions for each fixed magnetic order. We do not optimize the volume for the different configurations but maintain that of the G-type unit cell. For the  $R$  phase, G-type antiferromagnetic ordering is the most stable magnetic configuration across the whole strain range, consistent with bulk. In contrast, we find that in the  $T$  phase, G-type and C-type are nearly degenerate, with C-type being slightly lower in energy; for example, at 6% strain, the difference is 6 meV per formula unit<sup>30</sup>. In both G- and C-type, neighboring Fe moments within  $(001)_{\text{PS}}$  are antiferromagnetically aligned, but whereas for G-type neighboring moments are also antialigned in the out-of-plane direction, they are ferromagnetically aligned for C-type. A-type ordering, with parallel orientation of all magnetic moments within the same  $(001)_{\text{PS}}$  plane but alternating order in the perpendicular direction, is strongly unfavorable.

To further quantify this, we map the calculated total energies onto a nearest neighbor Heisenberg model where  $E = -\frac{1}{2}\sum_{ij}J_{ij}S_iS_j$ , and calculate the magnetic coupling constants  $J_{ij}$  for  $S_i = \pm\frac{5}{2}$ . We distinguish between in-plane coupling,  $J_{\text{in}}$ , and out-of-plane coupling  $J_{\text{out}}$ . For the  $T$ -phase at 6% strain, we find  $J_{\text{in}} = -10 \text{ meV}$  and  $J_{\text{out}} = 0.48 \text{ meV}$ , whereas for the  $R$ -phase at 1% strain,  $J_{\text{in}} = -9.8 \text{ meV}$  and  $J_{\text{out}} = -7.6 \text{ meV}$ . This shows that the increased distance between Fe atoms along  $[001]_{\text{PS}}$  in the high strain regime strongly reduces the magnetic coupling strength in that direction, leading to the very similar energies of C- and G-type magnetic order. The weak magnetic coupling between adjacent  $(001)_{\text{PS}}$  planes is likely to significantly reduce the magnetic ordering temperature, in spite of the strong coupling within individual  $(001)_{\text{PS}}$  planes.

## IV. SUMMARY AND DISCUSSION

In summary, our calculations of the effect of strain on BFO reveal two distinct structures in the high and low strain regime with a discontinuous first-order transition between them at  $\sim 4.5\%$  compressive strain. We note that, as a result of the constraints imposed by coherence and epitaxy, both phases have the same space group symmetry; such phase transitions are known as *isosymmetric* and are necessarily first

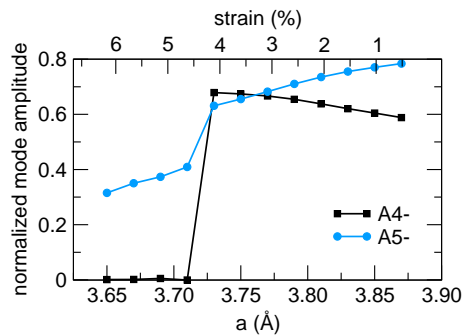


FIG. 4: Displacement mode amplitudes for dominant antiferrodistortive modes.  $A_{4-}$  and  $A_{5-}$  correspond to octahedral rotation and tilt, respectively.

order<sup>31</sup>. Isosymmetric transitions have also been demonstrated in pressure-induced transitions, as in  $\text{Fe}_{0.47}\text{NbS}_2$  and  $\alpha\text{-PbF}_2$ ,<sup>32,33</sup> or by temperature changes, as in  $\beta\text{-YbV}_4\text{O}_8$  and the fulleride  $\text{Sm}_{2.75}\text{C}_{60}$ ,<sup>34,35</sup>. Large volume changes appear to be characteristic. For example the pressure-induced spin-state transition in cerium is accompanied by a 16.5% volume change. Indeed BFO also undergoes a 9% change in volume from  $R$ - to  $T$ -phase (see Fig. 2b). To our knowledge this is the first example in the literature of a strain-induced isosymmetric phase transition. The recent work by Lisenkov *et al.*<sup>15</sup> showed that isosymmetric phase transitions in  $\text{BiFeO}_3$  films may also be induced by electric fields.

While such isosymmetry might enable the coexistence of the two phases recently reported in strained thin films<sup>11</sup>, we suggest that the low barrier between  $R$  and  $T$  phase, as shown in Fig. 1, is likely also a requirement. An  $R$  phase film with large compressive strain near the transition region can lower its energy significantly by relaxing to a slightly larger lattice parameter. This lattice expansion would normally create massive dislocations within the crystal, but because of the unusually flat energy surface near the transition region, it can be accommodated by the simultaneous development of  $T$  domains with decreased lattice parameter, incurring a relatively small energy penalty. This model for coexistence in BFO thin films can provide guidelines for identifying other systems with coexisting phases, namely the presence of an isosymmetric transition with a low energy barrier between phases. We also suggest that the isosymmetric nature of the transition facilitates the reversible movement of the boundary between  $R$  and  $T$  phases with an electric field<sup>11</sup>, as it obviates the need to change symmetry at the transition. The practical and technological implications of phase coexistence and morphotropic phase boundary-like behavior are being actively explored and we hope that the criteria suggested by our calculations will provide direction for future studies.

### Acknowledgments

We gratefully acknowledge support from the following: NSF Award Nos. DMR-0820404 and NIRT-0609377 (NAS and AJH) and Science Foundation Ireland through Contract

No. SFI-07/YI2/I1051 (CE). Travel support was provided by the International Center for Materials Research through the IMI Program of the NSF under Award No. DMR04-09848 (AJH). Computational resources used include the SGI Altix [Cobalt] system and the TeraGrid Linux Cluster [Mercury] at the National Center for Supercomputing Applications under

Grant No. DMR-0940420; CNSI Computer Facilities at UC Santa Barbara under NSF Grant No. CHE-0321368.; and facilities provided by the Trinity Centre for High Performance Computing. We thank R.J. Zeches, M.D. Rossell, L.W Martin, and R.Ramesh for helpful discussions.

- 
- <sup>1</sup> J. B. Neaton, C. Ederer, U. V. Waghmare, N. A. Spaldin, and K. M. Rabe, *Phys. Rev. B* **71**, 014113 (2005).
  - <sup>2</sup> C. Ederer and N. A. Spaldin, *Phys. Rev. B* **71**, 060401(R) (2005).
  - <sup>3</sup> J. Wang, J. B. Neaton, H. Zheng, V. Nagarajan, S. B. Ogale, B. Liu, D. Viehland, V. Vaithyanathan, D. G. Schlom, U. V. Waghmare, et al., *Science* **299**, 1719 (2003).
  - <sup>4</sup> T. Zhao, A. Scholl, F. Zavaliche, K. Lee, M. Barry, A. Doran, M. P. Cruz, Y. H. Chu, C. Ederer, N. A. Spaldin, et al., *Nat. Mater.* **5**, 823 (2006).
  - <sup>5</sup> D. Lebeugle, D. Colson, A. Forget, M. Viret, A. M. Bataille, and A. Gukasov, *Phys. Rev. Lett.* **100**, 227602 (2008).
  - <sup>6</sup> F. Kubel and H. Schmid, *Acta Crystallogr. B* **46**, 698 (1990).
  - <sup>7</sup> A. Biswas, M. Rajeswari, R. C. Srivastava, T. Venkatesan, R. L. Greene, Q. Lu, A. L. de Lozanne, and A. J. Millis, *Phys. Rev. B* **63**, 184424 (2001).
  - <sup>8</sup> D. G. Schlom, L. Q. Chen, C. B. Eom, K. M. Rabe, S. K. Streiffer, and J. M. Triscone, *Ann. Rev. Mater. Res.* **37**, 589 (2007).
  - <sup>9</sup> K. R. Balasubramaniam, S. Havelia, P. A. Salvador, H. Zheng, and J. F. Mitchell, *Appl. Phys. Lett.* **91**, 232901 (2007).
  - <sup>10</sup> H. Béa, B. Dupé, S. Fusil, R. Mattana, E. Jacquet, B. Warot-Fonrose, F. Wilhelm, A. Rogalev, S. Petit, V. Cros, et al., *Phys. Rev. Lett.* **102**, 217603 (2009).
  - <sup>11</sup> R. J. Zeches, M. D. Rossell, J. X. Zhang, A. J. Hatt, Q. He, C.-H. Yang, A. Kumar, C. H. Wang, A. Melville, C. Adamo, et al., *Science* **326**, 977 (2009).
  - <sup>12</sup> C. Ederer and N. A. Spaldin, *Phys. Rev. Lett.* **95**, 257601 (2005).
  - <sup>13</sup> D. Ricinschi, K.-Y. Yun, and M. Okuyama, *J. Phys. Condens. Mat.* **18**, L97 (2006).
  - <sup>14</sup> K. Y. Yun, D. Ricinschi, T. Kanashima, and M. Okuyama, *Appl. Phys. Lett.* **89**, 192902 (2006).
  - <sup>15</sup> S. Lisenkov, D. Rahmedov, and L. Bellaiche, *Phys. Rev. Lett.* **103**, 047204 (2009).
  - <sup>16</sup> G. Kresse and J. Furthmüller, *Phys. Rev. B* **54**, 11169 (1996).
  - <sup>17</sup> G. Kresse and D. Joubert, *Phys. Rev. B* **59**, 1758 (1999).
  - <sup>18</sup> R. D. King-Smith and D. Vanderbilt, *Phys. Rev. B* **47**, 1651 (1993).
  - <sup>19</sup> D. Vanderbilt and R. D. King-Smith, *Phys. Rev. B* **48**, 4442 (1993).
  - <sup>20</sup> D. H. Kim, H. N. Lee, M. D. Biegalski, and H. M. Christen, *Appl. Phys. Lett.* **92**, 012911 (2008).
  - <sup>21</sup> C. J. M. Daumont, S. Farokhipoor, A. Ferri, J. C. Wojdeł, J. Íñiguez, B. J. Kooi, and B. Noheda (2009), arXiv/0911.4502.
  - <sup>22</sup> C. Ederer and N. A. Spaldin, *Phys. Rev. B* **71**, 224103 (2005).
  - <sup>23</sup> A. A. Belik, M. Azuma, T. Saito, Y. Shimakawa, and M. Takano, *Chem. Mater.* **17**, 269 (2005).
  - <sup>24</sup> A. A. Belik, S. Iikubo, K. Kodama, N. Igawa, S.-i. Shamoto, S. Niitaka, M. Azuma, Y. Shimakawa, M. Takano, F. Izumi, et al., *Chem. Mater.* **18**, 798 (2006).
  - <sup>25</sup> A. T. Zayak, X. Huang, J. B. Neaton, and K. M. Rabe, *Phys. Rev. B* **74**, 094104 (2006).
  - <sup>26</sup> A. J. Hatt and N. A. Spaldin, *Eur. Phys. J. B* **71**, 435 (2009).
  - <sup>27</sup> D. Lebeugle, D. Colson, A. Forget, and M. Viret, *Appl. Phys. Lett.* **91**, 022907 (2007).
  - <sup>28</sup> H. W. Jang, S. H. Baek, D. Ortiz, C. M. Folkman, R. R. Das, Y. H. Chu, P. Shafer, J. X. Zhang, S. Choudhury, V. Vaithyanathan, et al., *Phys. Rev. Lett.* **101**, 107602 (2008).
  - <sup>29</sup> B. Campbell, H. Stokes, D. Tanner, and D. Hatch, *J. Appl. Cryst.* **39**, 607 (2006).
  - <sup>30</sup> This is in apparent contradiction to Ref. 10, where room temperature G-type AFM order is reported for BFO films on LaAlO<sub>3</sub> substrates. However, the strain in the experiment it is roughly 4%, and we therefore do not expect exact agreement with predictions for the 6% strain case.
  - <sup>31</sup> A. G. Christy, *Acta Crystallogr. B* **51**, 753 (1995).
  - <sup>32</sup> L. Ehm, K. Knorr, L. Peters, S. Rath, and W. Depmeier, *J. Alloy. Compd.* **429**, 82 (2007).
  - <sup>33</sup> J. Haines, J. M. Léger, and O. Schulte, *Phys. Rev. B* **57**, 7551 (1998).
  - <sup>34</sup> J. Arvanitidis, K. Papagelis, S. Margadonna, K. Prassides, and A. N. Fitch, *Nature* **425**, 599 (2003).
  - <sup>35</sup> K. Friese, Y. Kanke, A. N. Fitch, and A. Grzechnik, *Chem. Mater.* **19**, 4882 (2007).